Laminar and Turbulent Simulations of Several TVD Schemes in Two-Dimensions – Part III

Edisson S. G. Maciel

***Abstract*—**This work, third of this study, describes three numerical tools to perform perfect gas simulations of the laminar and turbulent viscous flow in two-dimensions. The Roe, Steger and Warming, and Hughson and Beran schemes, in their TVD ("Total Variation Diminishing") formulations, are implemented to accomplish the numerical simulations. The Navier-Stokes equations, on a finite volume context and employing structured spatial discretization, are applied to solve the supersonic flow along a ramp in two-dimensions. Three turbulence models are applied to close the system, namely: Cebeci and Smith, Baldwin and Lomax and Sparlat and Allmaras. The second-order versions of the Roe and Steger and Warming schemes are obtained from a "MUSCL" extrapolation procedure. The convergence process is accelerated to the steady state condition through a spatially variable time step procedure, which has proved effective gains in terms of computational acceleration (see Maciel). The results have shown that the Roe scheme yields the best results in terms of the prediction of the shock angle at the ramp. Moreover, the wall pressure distribution is better predicted by the Steger and Warming scheme.

***Keywords*—**Laminar and turbulent flows, TVD algorithms, Cebeci and Smith turbulence model, Baldwin and Lomax turbulence model, Sparlat and Allmaras turbulence model.

I. Introduction

CONVENTIONAL non-upwind algorithms have been used extensively to solve a wide variety of problems ([1]). Conventional algorithms are somewhat unreliable in the sense that for every different problem (and sometimes, every different case in the same class of problems) artificial dissipation terms must be specially tuned and judicially chosen for convergence. Also, complex problems with shocks and steep compression and expansion gradients may defy solution altogether.

Upwind schemes are in general more robust but are also more involved in their derivation and application. Some upwind schemes that have been applied to the Euler equations are, for example, [2-4]. Some comments about these methods are reported below:

[2] presented a work that emphasized that several numerical schemes to the solution of the hyperbolic conservation equations were based on exploring the information obtained in the solution of a sequence of Riemann problems. It was verified that in the existent schemes the major part of these information was degraded and that only certain solution aspects were solved. It was demonstrated that the information could be preserved by the construction of a matrix with a certain "U property". After the construction of this matrix, its eigenvalues could be considered as wave velocities of the Riemann problem and the UL-UR projections over the matrix's eigenvectors would be the jumps which occur between intermediate stages.

[3] developed a method that used the remarkable property that the nonlinear flux vectors of the inviscid gasdynamic equations in conservation law form were homogeneous functions of degree one of the vector of conserved variables. This property readily permitted the splitting of the flux vectors into subvectors by similarity transformations so that each subvector had associated with it a specified eigenvalue spectrum. As a consequence of flux vector splitting, new explicit and implicit dissipative finite-difference schemes were developed for first-order hyperbolic systems of equations.

[4] proposed an explicit, second order accurate in space, TVD scheme to solve the Euler equations in axis-symmetrical form, applied to the studies of the supersonic flow around a sphere and the hypersonic flow around a blunt body. The scheme was based on the modified flux function approximation of [5] and its extension from the two-dimensional space to the axis-symmetrical treatment was developed. Results were compared to the [6] algorithm's solutions. High resolution aspects, capability of shock capture and robustness properties of this TVD scheme were investigated.

This work, third of this study, describes three numerical tools to perform perfect gas simulations of the laminar and turbulent viscous flow in two-dimensions. The [2], the [3], and the [4] schemes, in its TVD versions, are implemented to accomplish the numerical simulations. The Navier-Stokes equations, on a finite volume context and employing structured spatial discretization, are applied to solve the supersonic flow along a ramp in two-dimensions. Three turbulence models are applied to close the system, namely: [7-9]. The second-order versions of the [2-3] schemes are obtained from a "MUSCL" extrapolation procedure. The convergence process is accelerated to the steady state condition through a spatially variable time step procedure, which has proved effective gains

Edisson S. G. Maciel works as a post-doctorate researcher at ITA (Aeronautical Technological Institute), Aeronautical Engineering Division – Praça Marechal do Ar Eduardo Gomes, 50 – Vila das Acácias – São José dos Campos – SP – Brazil – 12228-900 (corresponding author, phone number: +55 012 99165-3565; e-mail: edisavio@edissonsavio.eng.br).

in terms of computational acceleration (see [10-11]). The results have shown that the [2] scheme yields the best results in terms of the prediction of the shock angle at the ramp. Moreover, the wall pressure distribution is better predicted by the [3] scheme.

For an introduction about the motivation of this work, third part of this study, the reader is encouraged to read the first part of this work [12].

II. Navier-Stokes Equations

The flow is modeled by the Navier-Stokes equations, which express the conservation of mass and energy as well as the momentum variation of a viscous, heat conducting and compressible media, in the absence of external forces. These equations are described in detail in [12]. The reader is encouraged to read this reference aiming better understand of the present study.

III. TVD Algorithms

The description of the convective algorithms of [2-4] is presented in [13-16] and the reader is encouraged to read these papers to become familiar with all numerical schemes, and with the MUSCL approach. Hereafter, this paper will present the viscous formulation of both numerical schemes.

The viscous vectors are calculated with the gradients of the conserved and primitive variables keeping constant in each volume and the application of the Green's theorem to change from a volume integral to a surface integral.

The time integration is performed by a time splitting method, which divides the integration in two parts, each one associated with a spatial coordinate direction.

The numerical flux vector of the [2] scheme, for instance, is defined by, at the (i+1/2,j) interface:

$$F^{l}_{i+1/2,j} = \left[\left(E^{l}_{e_{i+1/2,j}} - E^{l}_{v_{i+1/2,j}}\right)h_x + \left(F^{l}_{e_{i+1/2,j}} - F^{l}_{v_{i+1/2,j}}\right)h_y\right]V_{i+1/2,j} + 0.5D^{l}_{Roe}, \quad (1)$$

where: E_e and F_e are the convective or Euler flux vectors, E_v and F_v are the viscous flux vectors, l varies from 1 to 4 (two-dimensional space), hx and hy are the metric terms, Vi+1/2,j is the interface volume, and D_{Roe} is the Roe's dissipation function, defined in [14, 16]. The Euler vectors are defined by the convective contributions of the numerical schemes.

The viscous vectors are calculated with the gradients of the conserved and primitive variables keeping constant in each volume and the application of the Green's theorem to change from a volume integral to a surface integral.

The time integration is performed by a time splitting method, which divides the integration in two parts, each one associated with a spatial coordinate direction. Therefore, to the ξ direction, one has:

$$\Delta Q^{*}_{i,j} = -\frac{\Delta t_{i,j}}{V_{i,j}}\left(F^{n}_{i+1/2,j} - F^{n}_{i-1/2,j}\right); \quad Q^{*}_{i,j} = Q^{n}_{i,j} + \Delta Q^{*}_{i,j}; \quad (2)$$

and to the η direction, one has:

$$\Delta Q^{n+1}_{i,j} = -\frac{\Delta t_{i,j}}{V_{i,j}}\left(F^{*}_{i,j+1/2} - F^{*}_{i,j-1/2}\right); \quad Q^{n+1}_{i,j} = Q^{*}_{i,j} + \Delta Q^{n+1}_{i,j}. \quad (3)$$

IV. Turbulence Models

The problem of the turbulent simulation is in the calculation of the Reynolds stress. Expressions involving velocity fluctuations, originating from the average process, represent six new unknowns. However, the number of equations keeps the same and the system is not closed. The modeling function is to develop approximations to these correlations. In this work, three turbulence models are studied: [7-8], algebraic ones, and [9], an one-equation model. To details of the present implementation, the reader is encouraged to read [12, 17].

V. Spatially Variable Time Step

The basic idea of the spatially variable time step procedure consists in keeping constant the CFL number in all calculation domain, allowing, hence, the use of appropriated time steps to each specific mesh region during the convergence process. In this work, a convective + diffusive option of spatially variable time step calculated at each iteration was studied. Details of the present implementation, see [12].

VI. Initial and Boundary Conditions

A. Initial Condition

Freestream values, at all grid cells, are adopted for all flow properties as initial condition, as suggested by [18].

B. Boundary Conditions

The boundary conditions are basically of three types: solid wall, entrance, and exit. These conditions are implemented in ghost cells. Details of the present implementation, see [12].

VII. Results

One problem was studied in this work, namely: the viscous supersonic flow along a ramp geometry. The ramp configuration is detailed as also the type of boundary contours. These configuration characteristics are described in Figs. 1 and 2.

Numerical experiments were run on a Notebook computer with Intel Core i7 processor of 2.3GHz of clock and 8.0 GBytes of RAM. The criterion adopted to reach the steady state was to consider a reduction of three (3) orders of magnitude in the value of the maximum residual in the calculation domain, a typical CFD community criterion. The maximum residual is defined as the maximum value obtained from the discretized equations in the overall domain, considering all conservation equations. The initial conditions to the ramp problem are described in Tab. 1.

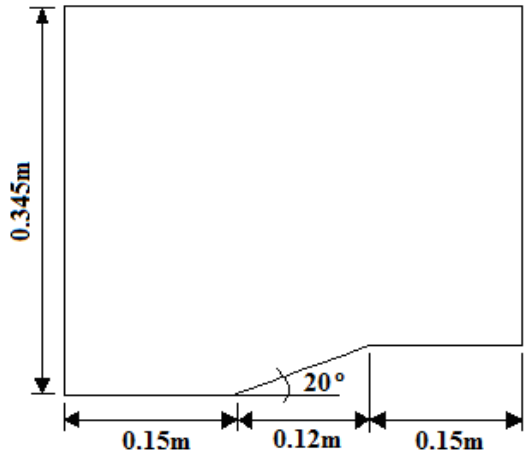

Figure 1. Ramp Configuration.

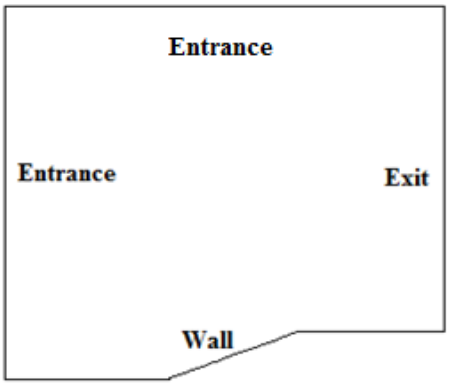

Figure 2. Ramp Computational Domain.

Table 1. Initial Conditions to the Studied Problem.

Problem:	Property:	Value:
Ramp	Freestream Mach, M∞	2.0
	Attack angle, °	0.0
	Ratio of specific heats, γ	1.4

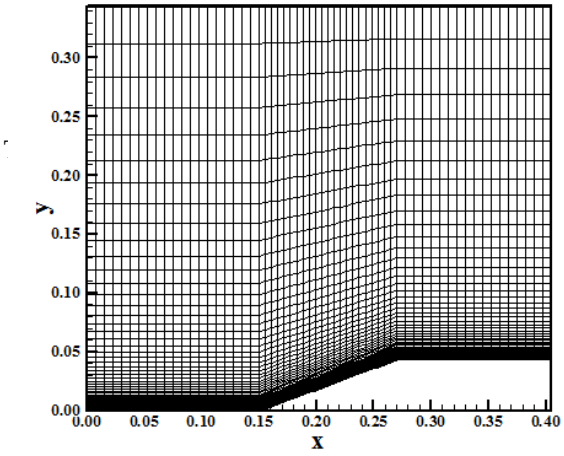

Figure 3. Ramp Viscous Mesh.

Figure 3 exhibits the mesh employed in the calculation of the viscous flow to the ramp problem. An exponential stretching of 10.0% was applied close to the wall, in the η direction, to capture the viscous phenomena.

Table 2. Number of Cells and Nodes for the Ramp Problem.

Problem:	Number of rectangular cells:	Number of nodes:
Ramp	3,540	3,660

The Reynolds number is equal to 1.613×10^5, a turbulent flow. Three turbulence models will be studied, namely: [7-9]. Two algebraic and an one-equation models are implemented.

The number of cells and nodes for the ramp problem are presented in Tab. 2. A mesh of 61x60 nodes, in a finite difference context, is employed.

A. Laminar Viscous Results

TVD Results. For the TVD results, a minmod non-linear limiter was employed in the [2-3] schemes. Figures 4 to 6 exhibit the pressure contours obtained by the [2-4] schemes. The [2] solution presents a weak shock ahead of the ramp corner. This shock wave is formed far ahead the ramp corner. The [3-4] solutions also present a weak shock wave, but less extent than the [2] scheme.

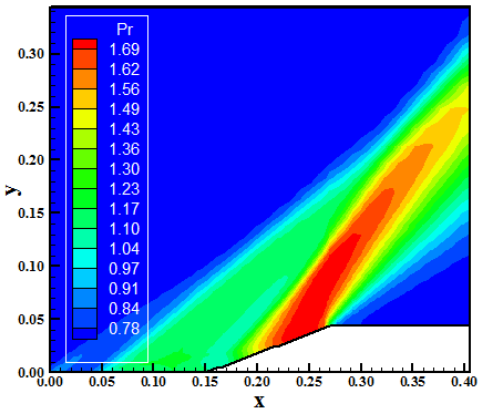

Figure 4. Pressure contours (Roe-TVD).

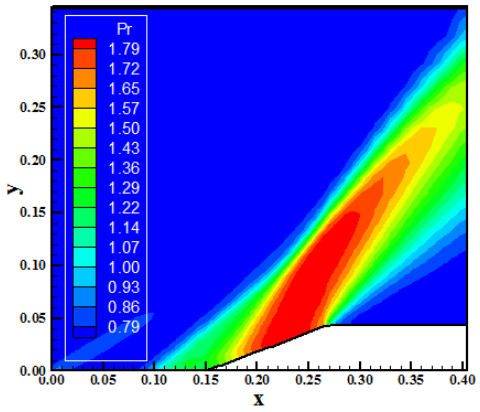

Figure 5. Pressure contours (SW-TVD).

The pressure field is more severe in the solution obtained by the [3] scheme, indicating this one as more conservative.

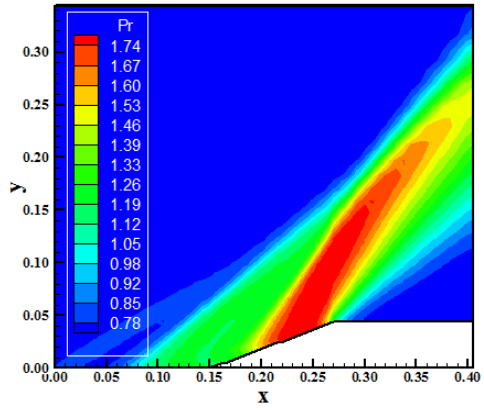

Figure 6. Pressure contours (HB-TVD).

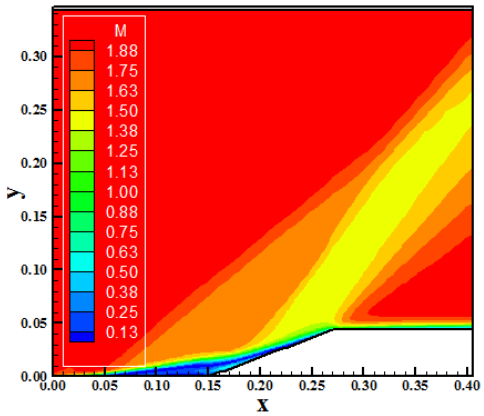

Figure 7. Mach number contours (Roe-TVD).

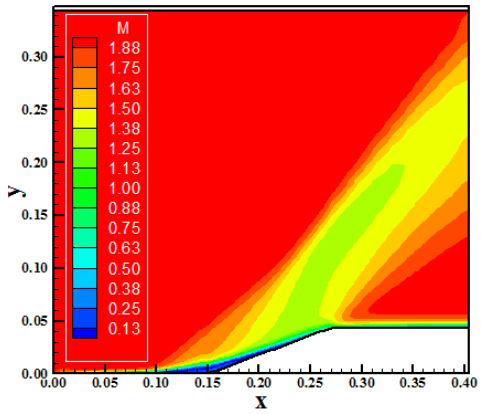

Figure 8. Mach number contours (SW-TVD).

Figures 7 to 9 show the Mach number contours obtained by the [2-4] algorithms. All solutions present a significant region of the detached boundary layer. However, the [2] solution indicates a largest region of detached boundary layer.

Figure 10 shows the wall pressure distributions generated by the [2-4] schemes in their TVD versions. All solutions capture the circulation bubble formation, resulting from the boundary layer detachment. The [3] solution presents a more discrete circulation bubble formation.

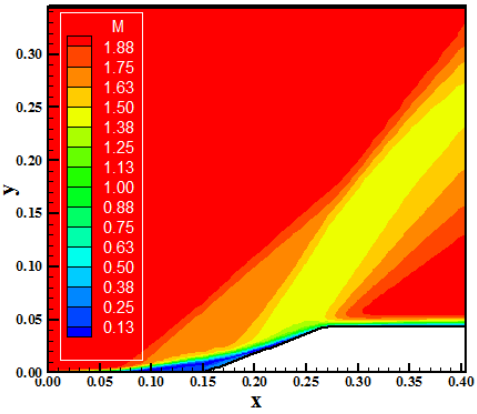

Figure 9. Mach number contours (HB-TVD).

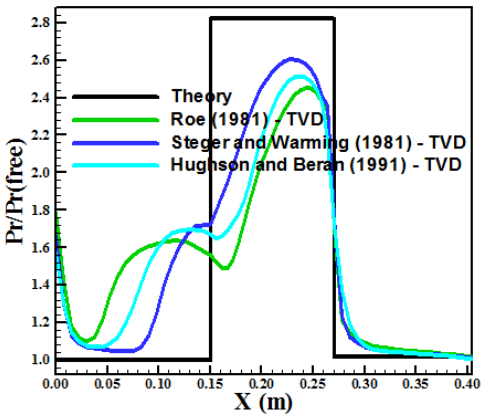

Figure 10. Wall pressure distributions.

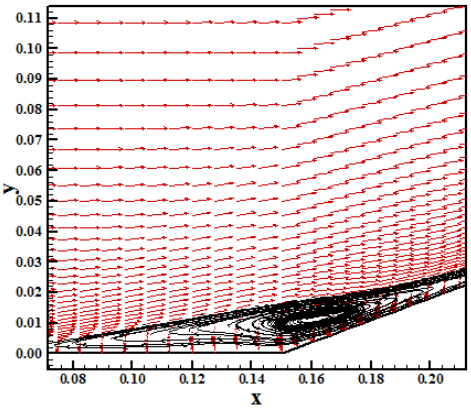

Figure 11. Circulation bubble (Roe-TVD).

Figures 11 to 13 presents the formation of circulation bubble closes to the ramp corner obtained by [2-4] schemes. The circulation bubble obtained by the [2] scheme is the largest.

As a resume of the present simulations, the [3] scheme was more conservative, although the [2] scheme was more correct in physical terms, representing more accurately the flow

physics.

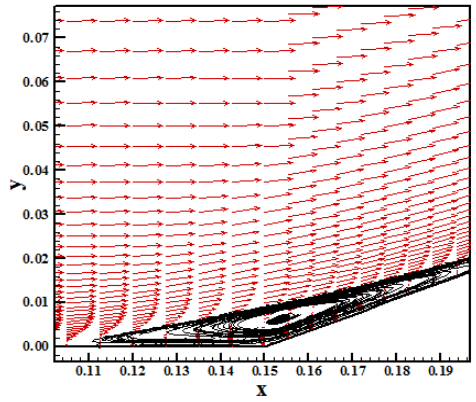

Figure 12. Circulation bubble (SW-TVD).

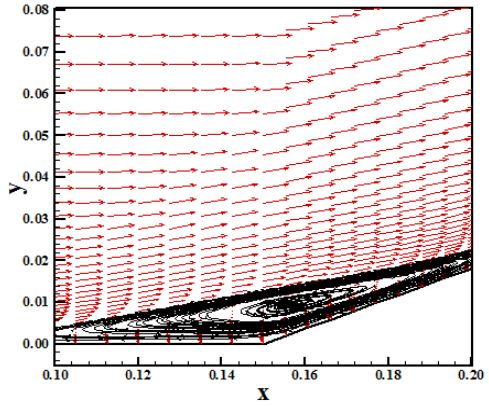

Figure 13. Circulation bubble (HB-TVD).

B. Turbulent Viscous Results

Cebeci and Smith TVD Results. Figures 14 to 16 show the pressure contours obtained by the [2-4] schemes, respectively, as using the [7] turbulence model. All solutions practically ignore the existence of the weak shock ahead of the ramp corner. It indicates that the boundary layer detachment is negligible in all solutions and that the circulation bubble is reduced in size. The pressure field generated by the [4] scheme is the most severe.

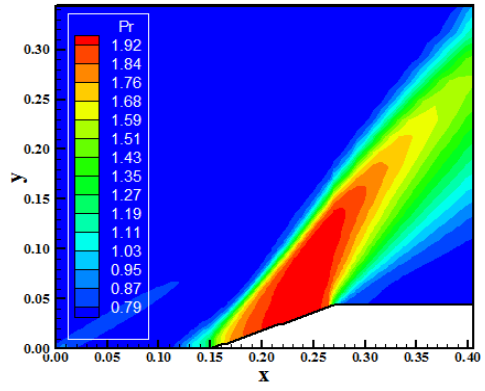

Figure 14. Pressure contours (Roe-CS).

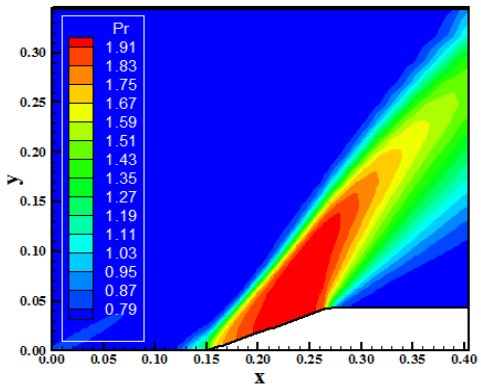

Figure 15. Pressure contours (SW-CS).

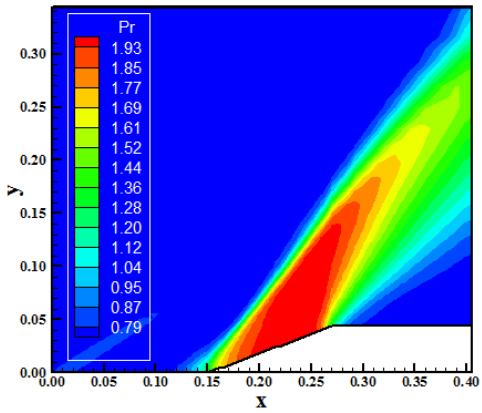

Figure 16. Pressure contours (HB-CS).

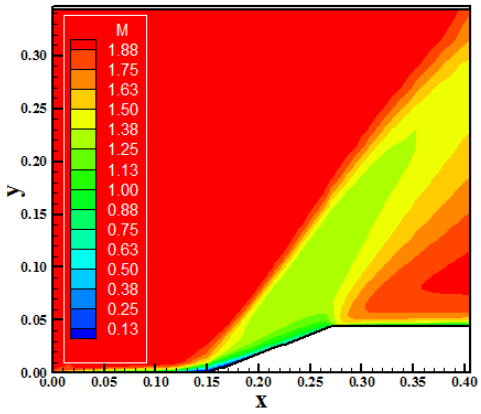

Figure 17. Mach number contours (Roe-CS) .

Figures 17 to 19 exhibit the Mach number contours generated by the [2-4] numerical algorithms, as using the [7] turbulence model. As can be observed, the boundary layer detachment is reduced in relation to the other results aforementioned for all algorithms. The circulation bubble is much more reduced.

Figure 20 exhibits the wall pressure distributions obtained by the [2-4] algorithms, as using the [7] turbulence model. As can be observed, all solutions are very similar and agree better

with the theoretical solution than in the laminar cases. The expansion fan pressure is better predicted by the [4] algorithm.

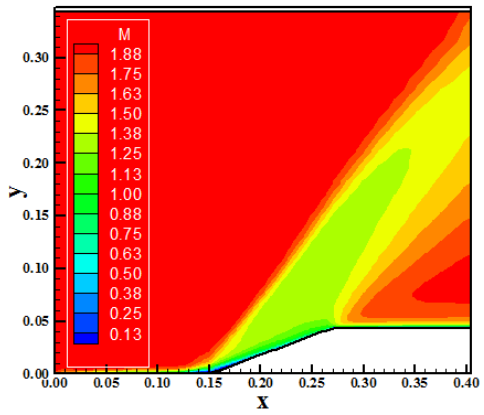

Figure 18. Mach number contours (SW-CS).

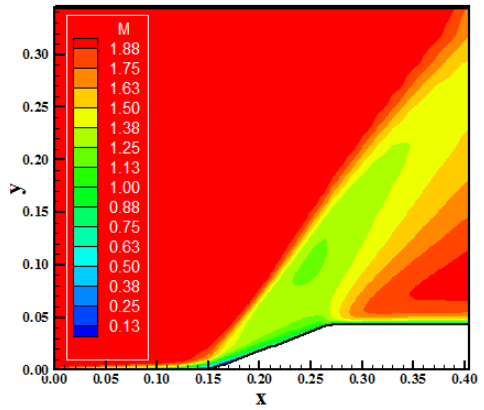

Figure 19. Mach number contours (HB-CS).

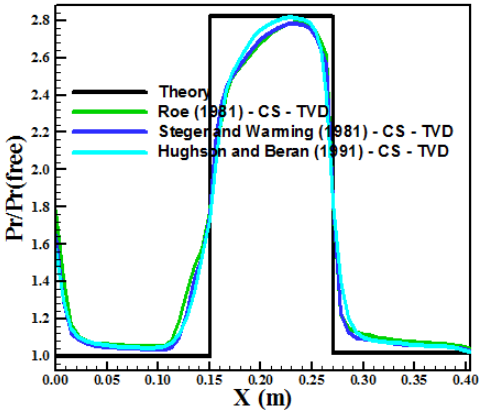

Figure 20. Wall pressure distributions.

Figures 21 to 23 show the circulation bubble formation close to the ramp corner. All solutions predicted a small circulation bubble, although that generated by the [2] scheme is the largest. In resume, as can be observed the [7] turbulence model predicts a more energized boundary layer. With it, the weak shock wave ahead of the ramp corner is negligible and the circulation bubble presents a discrete formation.

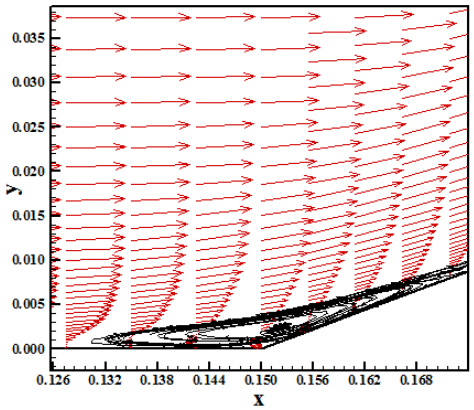

Figure 21. Circulation bubble (Roe-CS).

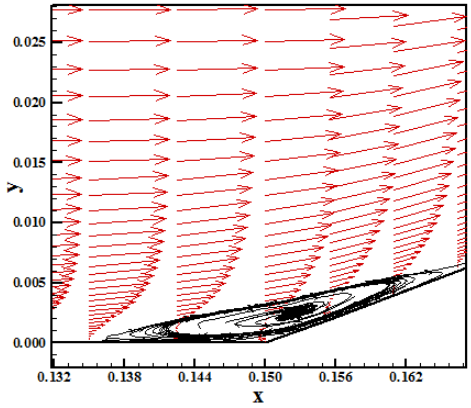

Figure 22. Circulation bubble (SW-CS).

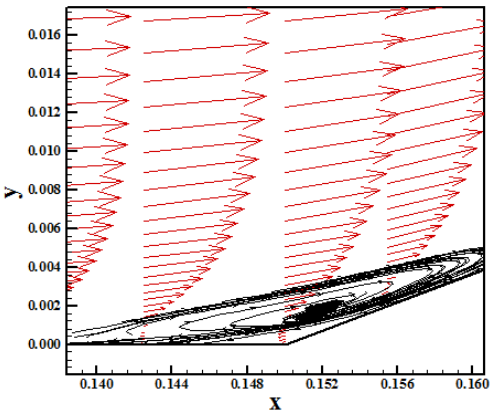

Figure 23. Circulation bubble (HB-CS).

Baldwin and Lomax TVD Results. Figures 24 to 26 exhibit the pressure contours obtained by the [2-4] schemes, respectively, as using the [8] turbulence model. A weak shock wave is formed ahead of the ramp corner in all solutions. It is important to remember that such weak shock wave is due to the boundary layer detachment which induces a false thick geometry at the ramp and the flow only see this thick geometry, originating the oblique shock wave. So, it is possible to distinguish that the effect of increasing boundary

layer thickness is more pronounced in the [2] solution than in the other solutions. It also induces the expected behavior of a larger circulation bubble formed at the former than at the latter. In terms of the pressure field, the [3] scheme again presents the most severe pressure field, characterizing this algorithm as more conservative.

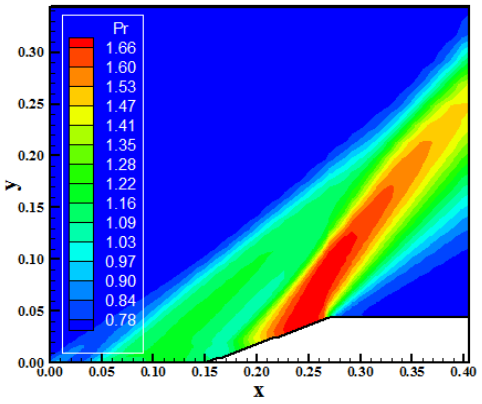

Figure 24. Pressure contours (Roe-BL).

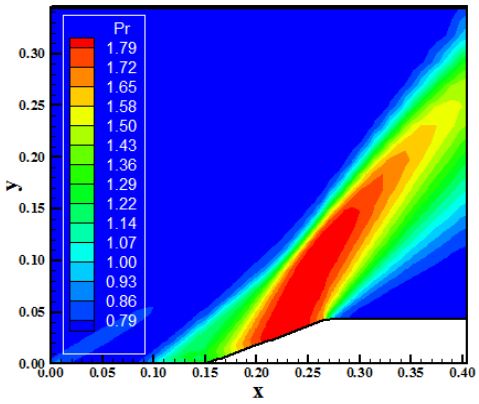

Figure 25. Pressure contours (SW-BL).

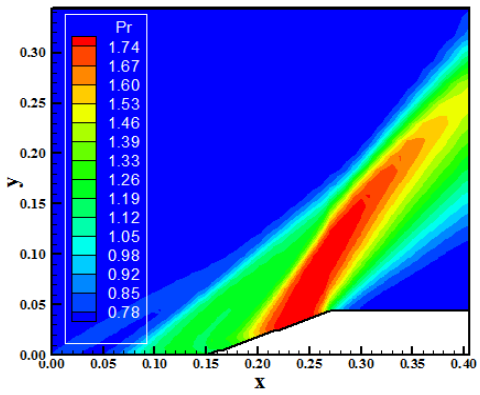

Figure 26. Pressure contours (HB-BL).

Figures 27 to 29 show the Mach number contours obtained by the [2-4] numerical algorithms, respectively, as using the [8] turbulence model. It is possible to observe that the boundary layer detachment is bigger in the [2] solution, with the consequent formation of a bigger circulation bubble than the other solutions. The Mach number field of all solutions is the same in quantitative terms, although in qualitative terms they differ substantially.

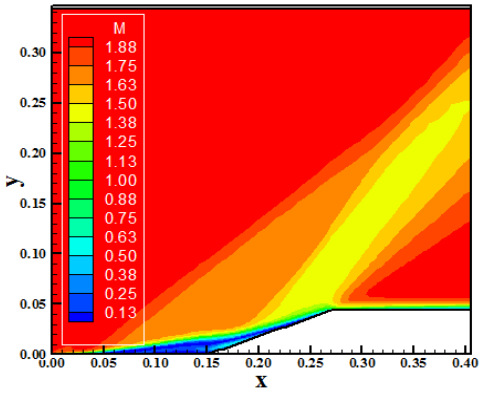

Figure 27. Mach number contours (Roe-BL).

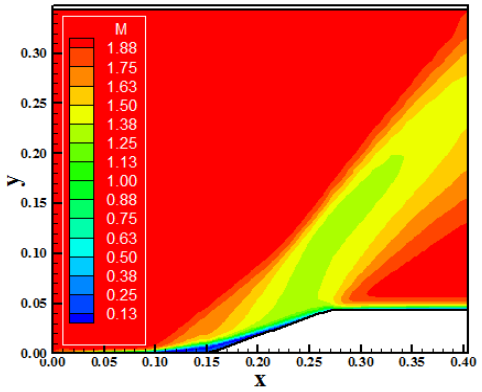

Figure 28. Mach number contours (SW-BL).

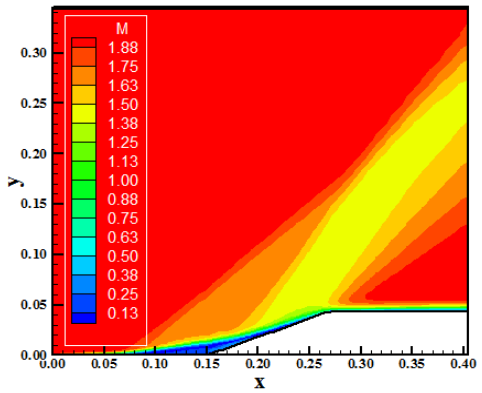

Figure 29. Mach number contours (HB-BL).

Figure 30 presents the wall pressure distributions generated by all algorithms. As noted, all solutions capture the circulation bubble formation closes to the ramp corner, but all solutions differs from the theoretical solution (both under-predict the shock plateau).

Figures 31 to 33 exhibit the circulation bubble formed close to the ramp corner generated by the [2-4] algorithms. The [2]

scheme presents the largest circulation bubble. In resume, the [8] turbulence model predicts a great extent region of boundary layer detachment and, consequently, bigger bubble size. The [8] model predicts bigger separation than the [7] model.

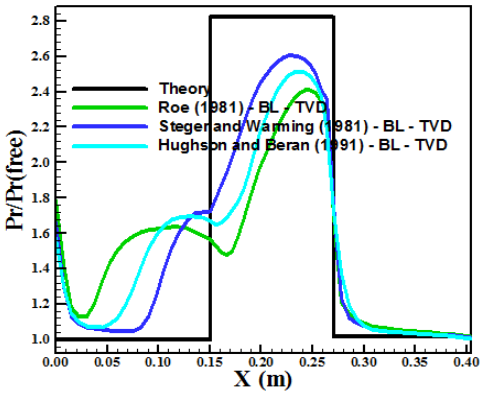

Figure 30. Wall pressure distributions.

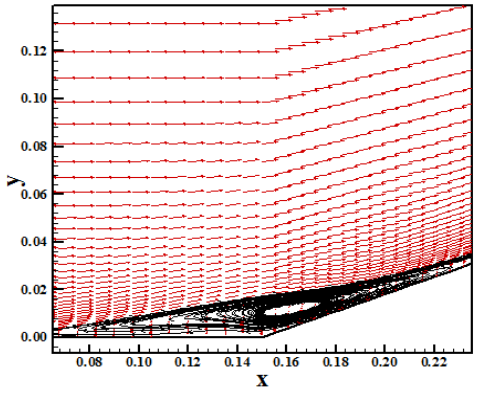

Figure 31. Circulation bubble (Roe-BL).

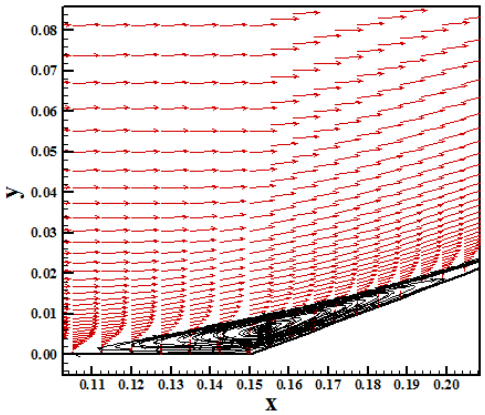

Figure 32. Circulation bubble (SW-BL).

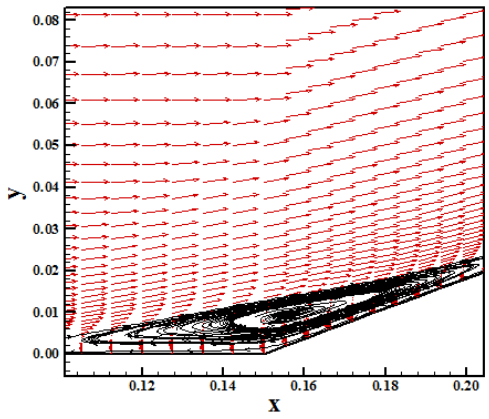

Figure 33. Circulation bubble (HB-BL).

Sparlat and Allmaras TVD Results. Figures 34 to 36 present the pressure contours obtained by the [2-4] schemes, respectively, as using the [9] turbulence model. Only the [2] solution captures the weak shock ahead of the ramp corner. The [3] solution captures a small boundary layer detachment, as also the [4] solution, which results in a negligible weak shock wave. The pressure field generated by the [3] scheme is again more severe than those generated by the [2, 4] schemes.

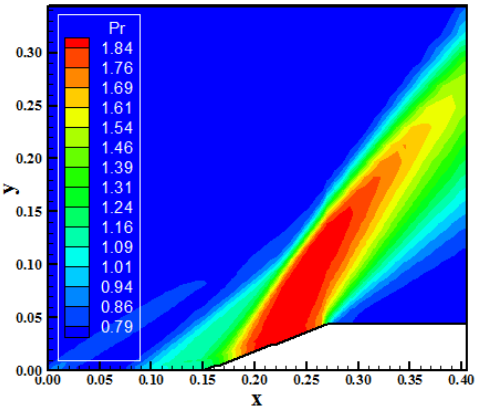

Figure 34. Pressure contours (Roe-SA).

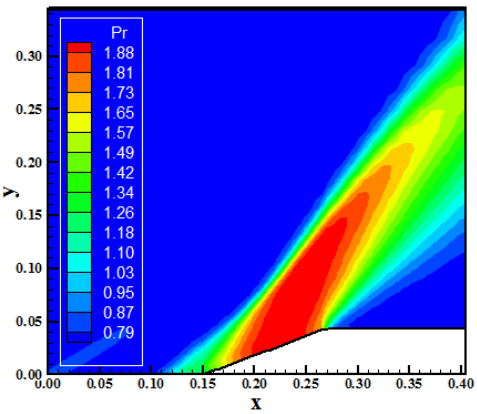

Figure 35. Pressure contours (SW-SA).

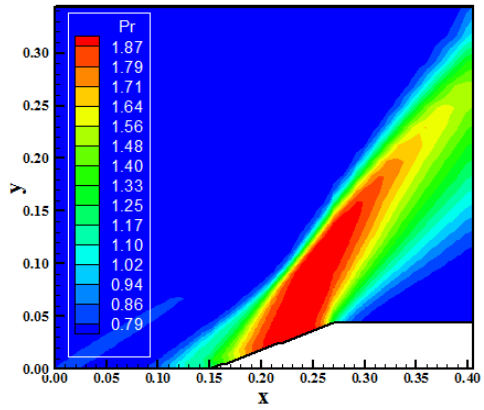

Figure 36. Pressure contours (HB-SA).

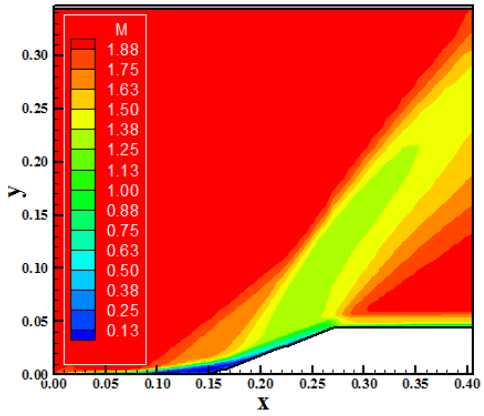

Figure 37. Mach number contours (Roe-SA).

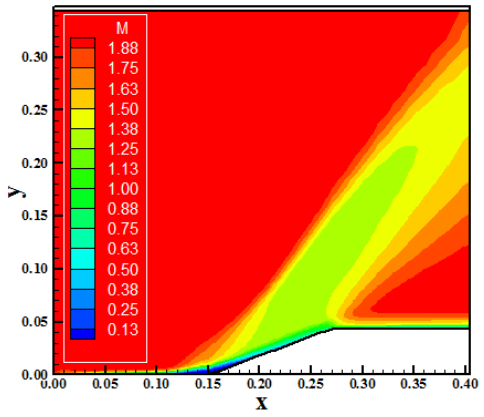

Figure 38. Mach number contours (SW-SA).

Figures 37 to 39 show the Mach number contours obtained by the [2-4] numerical schemes, respectively. The [2] solution again captures a bigger circulation bubble than the other solutions. In quantitative terms the solutions are the same, the difference existing in qualitative terms.

Figure 40 shows the wall pressure distributions obtained by the [2-4] algorithms. All solutions capture the circulation bubble at the ramp corner. Moreover, the pressure peak is close to the theoretical pressure plateau.

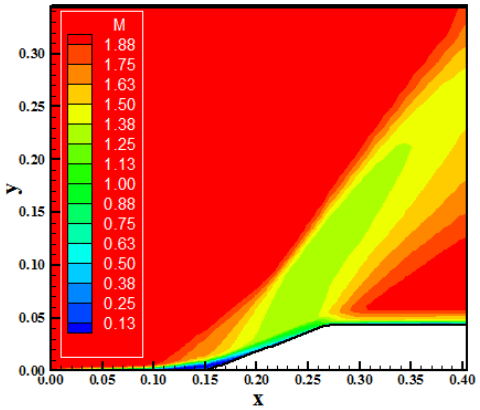

Figure 39. Mach number contours (HB-SA).

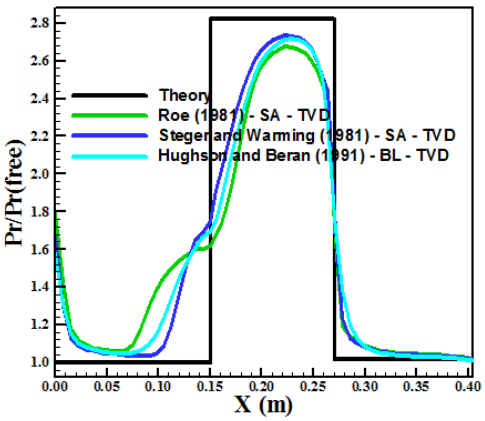

Figure 40. Wall pressure distributions.

It is important to be mentioned here that the best behavior to the pressure plateau was obtained by the [7] turbulence model in spite of the loss of physical meaning of the flow (loss of the circulation bubble formation).

Figures 41 to 43 exhibit the circulation bubble captured by the [2-4] schemeS, respectively, as using the [9] turbulence model. As can be seen, the [2] solution generates larger bubble region than the [3-4] solutions.

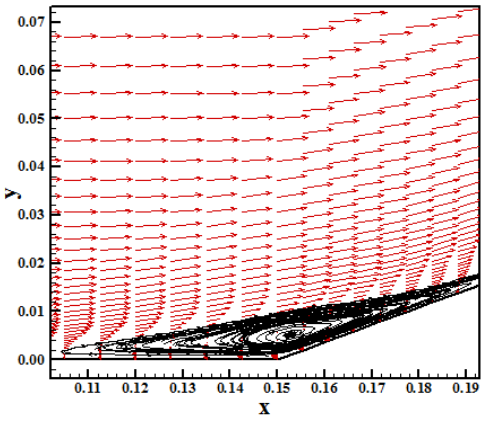

Figure 41. Circulation bubble (Roe-SA).

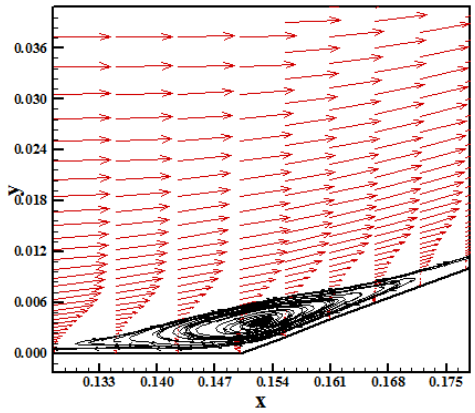

Figure 42. Circulation bubble (SW-SA).

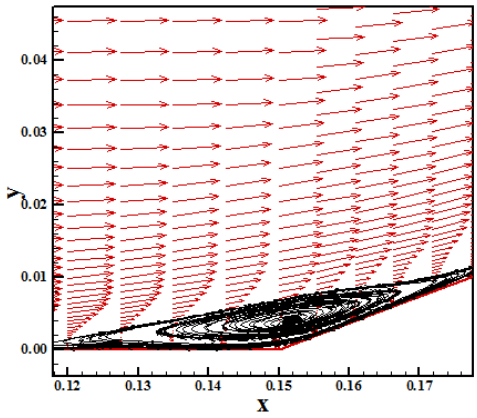

Figure 43. Circulation bubble (HB-SA).

In resume, the [9] turbulence model predicts a less extent region of boundary layer detachment and, consequently, minor bubble size. The [9] model, an one-equation model, predicts less severe separation than the [8] model.

C. *Quantitative Analysis*

One way to quantitatively verify if the solutions generated by each scheme are satisfactory consists in determining the shock angle of the oblique shock wave, β, measured in relation to the initial direction of the flow field. [19] (pages 352 and 353) presents a diagram with values of the shock angle, β, to oblique shock waves. The value of this angle is determined as function of the freestream Mach number and of the deflection angle of the flow after the shock wave, ϕ. To ϕ = 20º (ramp inclination angle) and to a freestream Mach number equals to 2.0, it is possible to obtain from this diagram a value to β equals to 53.0º. Using a transfer in Figures 4 to 6 (laminar, TVD), Figs. 14 to 26 (CS), Figs. 24 to 26 (BL), Figs. 34 to 36 (SA), it is possible to obtain the values of β to each scheme and to each studied case, as well the respective errors, shown in Tab. 3. It is possible to distinguish that the [2] scheme using the [8-9] turbulence models yields the best result with a zero value to the error. Hence, in terms of accuracy the [2] scheme is better than the other schemes.

Table 3. Values of the oblique shock wave angle.

Case	Lam., TVD	CS, TVD	BL, TVD	SA, TVD
Roe	51.5	51.4	53.0	53.0
Error (%)	2.83	3.02	0.00	0.00
SW	51.8	51.4	51.2	52.0
Error (%)	2.26	3.02	3.40	1.89
HB	55.5	51.5	54.0	54.0
Error (%)	4.72	2.83	1.89	1.89

Table 4. Computational data.

Case	Lam., TVD	CS, TVD	BL, TVD	SA, TVD
Roe	0.1	0.1	0.1	0.1
	42,756	15,238	50,141	29,273
SW	0.1	0.1	0.1	0.1
	25,777	12,079	25,758	18,902
HB	0.9	0.9	0.9	0.9
	4,177	1,412	4,177	2,437

Table 4 presents the computational data of the simulations. All schemes converged in three (3) orders. All second order solutions obtained from the use of MUSCL approach converged with a CFL number of 0.1. Oscillations and the non-convergence of the numerical scheme have occurred when numbers of CFL above 0.1 were used. It is important to highlight the excellent convergence of the [4] scheme, converging in all cases in less than 4,200 iterations.

VIII. Conclusions

This work, third of this study, describes three numerical tools to perform perfect gas simulations of the laminar and turbulent viscous flow in two-dimensions. The [2-4] schemes, in its TVD versions, are implemented to accomplish the numerical simulations. The Navier-Stokes equations, on a finite volume context and employing structured spatial discretization, are applied to solve the supersonic flow along a ramp in two-dimensions. Three turbulence models are applied to close the system, namely: [7-9]. The second-order versions of the [2-3] schemes are obtained from a "MUSCL" extrapolation procedure. The convergence process is accelerated to the steady state condition through a spatially variable time step procedure, which has proved effective gains in terms of computational acceleration (see [10-11]). The results have shown that the [2] scheme yields the best results in terms of the prediction of the shock angle at the ramp. Moreover, the wall pressure distribution is better predicted by the [3] scheme.

References

[1] P. Kutler, " Computation of Three-Dimensional, Inviscid Supersonic Flows", Lecture Notes in Physics, Vol. 41, 1975, pp. 287-374.

[2] P. L. Roe, "Approximate Riemann Solvers, Parameter Vectors, and Difference Schemes", Journal of Computational Physics, Vol. 43, 1981, pp. 357-372.

[3] J. L. Steger, and R. F. Warming, "Flux Vector Splitting of the Inviscid Gasdynamic Equations with Application to Finite-Difference Methods", Journal of Computational Physics, Vol. 40, 1981, pp. 263-293.
[4] M. C. Hughson, and P. S. Beran, "Analysis of Hyperbolic Blunt-Body Flows Using a Total Variation Diminishing (TVD) Scheme and the MacCormack Scheme", AIAA 91-3206-CP, 1991.
[5] A. Harten, "High Resolution Schemes for Hyperbolic Conservation Laws", Journal of Computational Physics, Vol. 49, 1983, pp. 357-393.
[6] R. W. MacCormack, "The Effect of Viscosity in Hypervelocity Impact Cratering", AIAA Paper 69-354**,** 1969.
[7] T. Cebeci, and A. M. O. Smith, "A Finite-Difference Method for Calculating Compressible Laminar and Turbulent Boundary Layers", Journal of Basic Engineering, Trans. ASME, Series B, Vol. 92, No. 3, 1970, pp. 523-535.
[8] B. D. Baldwin, and H. Lomax, "Thin Layer Approximation and Algebraic Model for Separated Turbulent Flows", AIAA Paper 78-257, 1978.
[9] P. R. Sparlat, and S. R. Allmaras, "A One-Equation Turbulence Mode for Arodynamic Flows", AIAA Paper 92-043, 1992.
[10] E. S. G. Maciel, "Analysis of Convergence Acceleration Techniques Used in Unstructured Algorithms in the Solution of Aeronautical Problems – Part I, Proceedings of the XVIII International Congress of Mechanical Engineering (XVIII COBEM), Ouro Preto, MG, Brazil, 2005.
[11] E. S. G. Maciel, "Analysis of Convergence Acceleration Techniques Used in Unstructured Algorithms in the Solution of Aerospace Problems – Part II", Proceedings of the XII Brazilian Congress of Thermal Engineering and Sciences (XII ENCIT), Belo Horizonte, MG, Brazil, 2008.
[12] E. S. G. Maciel, "Laminar and Turbulent Simulations of Several TVD Schemes in Two-Dimensions – Part I – Theory", Submitted to International Journal of Mathematics and Computers in Simulation (under review), 2014.
[13] E. S. G. Maciel, "Comparison Between the Yee, Warming and Harten and the Hughson and Beran High Resolution Algorithms in the Solution of the Euler Equations in Two-Dimensions – Theory", Proceedings of the XXVII Iberian Latin American Congress on Computational Methods in Engineering (XXVII CILAMCE), Belém Pará, Brazil, 2006.
[14] E. S. G. Maciel, "Comparison Among the First Order Upwind Algorithms of Roe, of Steger and Warming, of Van Leer and of Chakravarthy and Osher in the Solution of the Euler Equations in 2D – Theory", Proceedings of the VIII Symposium of Computational Mechanics (VIII SIMMEC), Belo Horizonte, MG, Brazil, 2008.
[15] E. S. G. Maciel, "Extension of the Steger and Warming and Radespiel and Kroll Algorithms to Second Order Accuracy and Implicit Formulation Applied to the Euler Equations in Two-Dimension – Theory, Proceedings of the VI National Congress of Mechanical Engineering (VI CONEM), Campina Grande, Paraíba, Brazi, 2010.
[16] E. S. G. Maciel, "Extension of the Roe and Van Leer Algorithms to Second Order Accuracy Applied to the Euler Equations in Two-Dimensions, Proceedings of the 12th Pan-American Congresso f Applied Mechanics (XII PACAM), Port of Spain, Trinidad, 2012.
[17] E. S. G. Maciel, "Laminar and Turbulent Simulations of Several TVD Schemes in Two-Dimensions – Part II", Submitted to the International Journal of Applied Mathematics and Informatics (under review), 2014.
[18] E. S. G. Maciel, "Simulação Numérica de Escoamentos Supersônicos e Hipersônicos Utilizando Técnicas de Dinâmica dos Fluidos Computacional", Doctoral Thesis, ITA, CTA, São José dos Campos, SP, Brazil, 2002.
[19] J. D. Anderson Jr., "Fundamentals of Aerodynamics", McGraw-Hill, Inc., EUA, 563p., 1984.

Edisson S. G. Maciel (F'14), born in 1969, february, 25, in Recife, Pernambuco. He is a Mechanical Engineering undergraduated by UFPE in 1992, in Recife, PE, Brazil; Mester degree in Thermal Engineering by UFPE in 1995, in Recife, PE, Brazil; Doctor degree in Aeronautical Engineering by ITA in 2002, in São José dos Campos, SP, Brazil; and Post-Doctor degree in Aeronautical Engineering by ITA in 2009, in São José dos Campos, SP, Brazil.

Actually, he is doing a new post-doctorate curse in Aerospace Engineering at ITA. The last researches are based on thermochemical non-equilibrium reentry simulations in Earth and thermochemical non-equilibrium entry simulations in Mars. They are: Maciel, E. S. G., and Pimenta, A. P., "Thermochemical Non-Equilibrium Reentry Flows in Two-Dimensions – Part I', WSEAS Transactions on Mathematics, Vol. 11, Issue 6, June, pp. 520-545, 2012; Maciel, E. S. G., and Pimenta, A. P., "Thermochemical Non-Equilibrium Entry Flows in Mars in Two-Dimensions – Part I', WSEAS Transactions on Applied and Theoretical Mechanics, Vol. 8, Issue 1, January, pp. 26-54, 2013; and he has three published books, the first one being: Maciel, E. S. G., "Aplicações de Algoritmos Preditor-Corretor e TVD na Solução das Equações de Euler e de Navier-Stokes em Duas Dimensões", Recife, PE, Editor UFPE, 2013. He is interested in the Magnetogasdynamic field with applications to fluid dynamics and in the use of ENO algorithms.